Effect of dispersion correction on the Au(1 1 1)-H_2O interface: A first-principles study

Cite as: J. Chem. Phys. **137**, 114709 (2012); https://doi.org/10.1063/1.4752235
Submitted: 21 March 2012 . Accepted: 22 August 2012 . Published Online: 21 September 2012

Roger Nadler, and Javier Fdez. Sanz

Effect of dispersion correction on the Au(1 1 1)-H_2O interface: A first-principles study

Roger Nadler[a] and Javier Fdez. Sanz
Department of Physical Chemistry, University of Seville, 41012 Seville, Spain

(Received 21 March 2012; accepted 22 August 2012; published online 21 September 2012)

A theoretical study of the H_2O-Au(1 1 1) interface based on first principles density functional theory (DFT) calculations with and without inclusion of dispersion correction is reported. Three different computational approaches are considered. First, the standard generalized gradient approximation (GGA) functional PBE is employed. Second, an additional energy term is further included that adds a semi-empirically derived dispersion correction (PBE-D2), and, finally, a recently proposed functional that includes van der Waals (vdW) interactions directly in its functional form (optB86b-vdW) was used to represent the state-of-the art of DFT functionals. The monomeric water adsorption was first considered in order to explore the dependency of geometry on the details of the model slab used to represent it (size, thickness, coverage). When the dispersion corrections are included the Au-H_2O interaction is stronger, as manifested by the smaller $d_{Au\text{-}O}$ and stronger adsorption energies. Additionally, the interfacial region between Au(1 1 1) slab surfaces and a liquid water layer was investigated with Born-Oppenheimer molecular dynamics (BOMD) using the same functionals. Two or three interfacial orientations can be determined, depending on the theoretical methodology applied. Closest to the surface, H_2O is adsorbed O-down, whereas further away it is oriented with one OH bond pointing to the surface and the molecular plane parallel to the normal direction. For the optB86b-vdW functional a third orientation is found where one H atom points into the bulk water layer and the second OH bond is oriented parallel to the metal surface. As for the water density in the first adsorption layer we find a very small increase of roughly 8%. From the analysis of vibrational spectra a weakening of the H-bond network is observed upon the inclusion of the Au(1 1 1) slab, however, no disruption of H-bonds is observed. While the PBE and PBE-D2 spectra are very similar, the optB86b-vdW spectrum shows that the H-bonds are even more weakened. © *2012 American Institute of Physics*. [http://dx.doi.org/10.1063/1.4752235]

I. INTRODUCTION

The metal-water interface is a classic in chemistry and enjoys growing attention from both experimentalists and theoreticians. Several extensive reviews cover the subject, giving a vast overview about interfacial interactions between water and metal surfaces.[1–3] Applications are found in several different fields, such as biological systems, electrochemistry, materials science, and solid-state chemistry, to name but a few. Despite the abundant theoretical and experimental work performed up to now, the exact nature of the adsorption of H_2O on different metal surfaces is still not fully uncovered.

The general picture of water adsorbed on hexagonally close-packed metal surfaces at low coverage is the one of water forming ice-like hexagonal bilayers with a $(\sqrt{3}\times\sqrt{3})R30^\circ$ periodicity showing flattened rings to conform to the substrate periodicity. Yet the increased accuracy of experimental methods leads to a revised picture of this description. On Pd(1 1 1) surfaces it was found that planar hexamer rings of nearly flat-lying water molecules form lace-like and rosette structures on the surface.[4] On Pt(1 1 1) surfaces 5- and 7-membered rings were reported,[5] and, finally, growth of 1D ice structure on Cu(1 1 0) surfaces occurs via pentagons.[6] A short review about the recent findings concerning the large number of structures of water on metal substrates was recently written by Carrasco *et al.*[7]

However, when the adsorption of the H_2O monomer is considered, theoretical calculations predict that H_2O is adsorbed nearly parallel to the surface at a distance of around 2.6 to 3 Å.[8–12] The largest and smallest adsorption energies differ by only 0.06 eV, which is owed to the very flat potential energy surface. It was reported earlier that surface size effects might play a role in the investigation of H_2O adsorption on face centered cubic (*fcc*) metal surfaces.[13–16] The conclusion of the discussion is that a super-cell surface should be large enough to minimize dipole interaction between periodic images. Furthermore, within the metal-water interface, weak van der Waals (vdW) interactions between surface metal atoms and water molecules have an undisputed influence on geometric properties and, although smaller, on energetics. Because of the unknown exact dependency on the exact correlation, current generalized gradient approximation (GGA) functionals used in density functional theory (DFT) do not account for those interactions. To address for such dispersion effects, they are included as a pair-wise force field to correct the long-range dispersion (DFT-D).[17–19] There is an ongoing improvement related to this kind of approach. Compared to

[a]Author to whom correspondence should be addressed. Electronic mail: rnadler@us.es.

the DFT-D2 version, where the force-field parameters are obtained empirically and the C_6 parameters are environment-independent,[17] the empiricism of newly developed force field parameters has been reduced and the C_6 parameters have been obtained in an environment-dependent fashion.[18,19] The most recent development in this sense is Grimme's DFT-D3 method[18] and the Tkatchenko-Scheffler (TS) approach.[19] Another approach is to replace the original correlation functional of a given exchange-correlation (xc) functional directly with a non-local correlation functional (vdW-DF).[20,21] Cicero *et al.* recently presented a study where they used the DFT-D2 approach to calculate the geometry of an H_2O molecule adsorbed on the Au(1 1 1) surface,[11] and Poissier *et al.* applied the vdW-DF approach on a Pd(1 1 1)-H_2O system.[15] The DFT-D2 approach might be problematic if used with the PBE functional, as it overestimates the water-water interaction by ∼13%, while the revised version[22] (RPBE) only does so by 6%.[23] Therefore, the RPBE would be a better choice to calculate metal-water interfaces, especially if additional adsorbates are included in the system.

The different methodologies may perform differently. Using the vdW-DF for the Pd-H_2O interface, Poissier *et al.* found that the Pd-O distance increases and also that the tilt angle obtained was larger when compared to calculations without correction for dispersion interactions.[15] In contrast, Cicero *et al.* observed that, in the case of the Au(1 1 1)-H_2O interaction, the $d_{\text{Au-O}}$ distance decreased by almost 0.3 Å when applying the PBE-D2 approach.[11] This is at variance of the behavior observed by Xue for H_2O adsorbed on gold clusters,[24] where the $d_{\text{Au-O}}$ distance was found to increase when the revised vdW-DF and vdW-DF2 functionals were applied.[25] However, the increased distances obtained with the vdW-DF and vdW-DF2 functionals are considered to be overestimated.[26,27] Therefore, it is desired to further improve this kind of functional. Klimeš *et al.* developed a vdW-DF variant based upon the optimized PBE functional (optPBE-vdW).[28] Particularly, if only the properties of the condensed phase of water are considered, then it is an interesting choice as it reproduces almost identically the dissociation energies of the water hexamer compared to those obtained with ΔCCSD(T) calculations. Unfortunately, it gives lattice constants for a wide range of solids that are rather large, although not as large as if the original revPBE-vdW functional were used.[21] Still, since it is widely accepted that dispersion effects play an important role in the description of the metal-water interactions,[29,30] application of dispersion corrected functionals is crucial, even more because their contribution becomes more elusive when such interactions are weak. There are also reports found in literature where the performance of dispersion corrected functionals, both vdW-DF[15] and DFT-D,[31] are critically analyzed, and further improvement of Kohn-Sham DFT is desired to obtain quantitatively accurate results for H-bonding liquids.[31,32] The recent vdW-DF functionals such as optB86b-vdW[21] are certainly one step in this direction.

Upon contact with a metal surface, liquid water will experience a layering with respect to the surface normal. X-ray experiments carried out by Toney *et al.*[33] even revealed that in the case of the Ag(1 1 1)-H_2O interface under an external potential, the density of the first layer is noticeably increased where the minimum is at the potential of zero charge (*pzc*) and is compressed by a factor of two at charged surfaces. Based on their finding they concluded that at a potential of +0.52 V above the *pzc*, the puckered, hexagonal ice-like structure collapses. Ataka *et al.* investigated the Au(1 1 1)-H_2O interface by surface-enhanced infrared spectroscopy.[34] They compared the effects of different types of anions on the stretching mode band, ν_{stretch}, of H_2O and finally concluded that ions that are co-adsorbed on the surface break hydrogen-bonding of the ice-like adsorption layer and change the arrangement of the H_2O molecules in the interface, thereby supporting the results of Toney *et al.* They do differ, however, in that Ataka *et al.* attributed the collapse and rearrangement to the ion-water interaction while Toney *et al.* ruled this possibility out and interpreted it as a consequence of the Ag-H_2O interaction. Ito reports that at hydrogen evolution potentials the mean distance between the O layer and an underlying Cu surface is 2.1 Å.[35] Such a distance makes it improbable that H_2O is adsorbed H-down as it was proposed by Toney *et al.* at negative potentials. There also exist experimental and theoretical reports where the authors were not able to reproduce the density increase as it was reported by Toney *et al.*[36–39] However, they do coincide with the layering of the water above the surface, although not to the same extent. For instance, Schnur and Gross performed *ab initio* molecular dynamics of a water bilayer over several noble metals.[39] For the Au(1 1 1)-H_2O interface they found that the initial bilayer structure ends up forming just one broad peak in the wall oxygen distribution function instead of two, resulting in a complete loss of the water bilayer structure, and, hence, a weak Au-water interaction. Also Cicero *et al.* reported a density increase within the first wetting layer compared to the liquid water density.[11]

Although water has been subject of various studies using DFT-D2,[17,31,40,41] the application of this methodology to metals has been awaited until recently due to the lack of parameters for some heavy metals that account correctly for the vdW interactions. Two reports propose parameters for the C_6 term of the dispersion correction, which are relatively similar,[42,43] however, they were obtained using thiols and aromatic molecules for which they perform close to experimental data. It is to be shown if DFT-D2 will reproduce the water-Au(1 1 1) interface correctly. In comparison, vdW-DF is free of such limitations as it does not rely on empirically determined parameters.

In this paper, we report a theoretical study of the Au(1 1 1)-H_2O interface based on first principles DFT calculations. These are carried out using the PBE functional, both in its standard form and adding semi-empirical dispersion corrections to it, according to the DFT-D2 scheme aforementioned. Furthermore, the optB86b-vdW functional is considered which includes the non-local correlation part in its functional form. As a first step, we have considered the interaction of the Au(1 1 1) surface with a water monomer and have estimated the binding energy and structure of the adsorbate on different super-cell models of the Au(1 1 1) surface, investigating the dependency of the adsorption parameters on slab size and thickness, as well as on coverage. As a second step, we have performed molecular dynamics (MD) simulations

on the Born-Oppenheimer surface, applying the same theoretical approaches as before. From the obtained trajectories, the properties of interfacial water have been examined. This analysis is based on the planar distribution functions $g(z)$, angular probability distribution functions $p(\varphi, z)$ and $p(\theta, z)$, determination of hydrogen bonds, and vibrational spectra.

II. METHODOLOGY

A. Models

First, using a $p(4 \times 4)$ super-cell surface, the influence of the slab thickness on the geometric and energetic adsorption parameters of the H_2O monomer was analyzed. A set of slabs was established, consisting of slabs with n layers, where $n = 4-8$. The lowest layer was not relaxed in order to avoid spurious drifts of the total system.

To investigate the dependency on the coverage, $p(2 \times 2)$ and $p(4 \times 4)$ 7-layer thick super-cells were considered. Larger models were shown to have a negligible impact on the adsorption geometry as well as on the adsorption energy of the monomer.[16] Thus, the following coverage was investigated: $\Theta = 1/16$, 1/8, and 1/4 ML. An illustration of how the molecules were placed on the $p(4 \times 4)$ super-cell is represented in Fig. 1. With four H_2O molecules adsorbed, the coverage is set to 1/4 ML. If the two glossy water molecules were removed, $\Theta = 1/8$ ML is obtained. Finally, leaving only one water molecule we reach the coverage $\Theta = 1/16$ ML. In all cases, a vacuum layer of at least 15 Å was introduced to avoid interactions between the two sides of a given slab.

All main calculations were performed applying three computational approaches. First, the GGA functional PBE was employed. It was also used together with the semi-classical dispersion correction proposed by Grimme,[17] which we label PBE-D2. The R and C_6 dispersion correction parameters for water were taken from the original work of Grimme[17] while for gold we used those suggested by Nguyen *et al.*[42] We should emphasize here that these parameters for Au are derived using an aromatic molecule. However, Cicero *et al.* reported reasonable results using these parameters.[11] To deal with possible screening effects that could occur when the Au parameters are applied to the whole slab, only the surface atoms are corrected for the dispersion forces.[44,45] It was shown that nonlocal screening reduces the C_6 term up to four times when the Lifshitz-Zaremba-Kohn theory is taken into account for the non-local Coulomb screening together with DFT corrected for dispersion interaction.[46] At least for the monomeric adsorption part, this approximation still leads to unsatisfactory results with the parameters used for the semi-empirical dispersion correction; consequently, only three slab thicknesses were calculated with this methodology ($n = 4$, 5, 6). Finally, the van der Waals functional optB86b-vdW[21] is used to represent a more sophisticated methodology available nowadays within the DFT framework to describe weak vdW interactions.

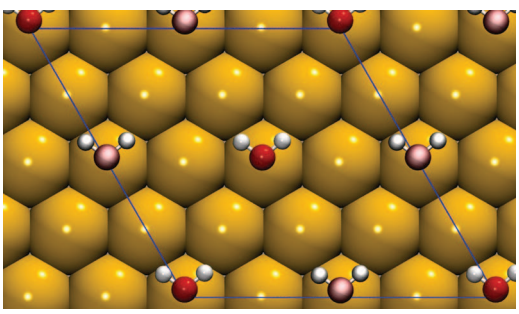

FIG. 1. Represented are the H_2O molecules on their optimized atop adsorption sites on a $p(4 \times 4)$ surface in order to model a coverage of 1/4 ML. The glossy water molecules were removed to obtain the coverage of 1/8 ML. The super-cell is outlined in blue. O atoms are in red, H atoms in white, and Au atoms in yellow.

For each methodology the lattice constant a_0 for Au(1 1 1) was optimized. The PBE lattice constant was calculated to be 4.174 Å; for the PBE-D2 it resulted in it being slightly smaller at 4.164 Å. Using the optB86b-vdW functional we yielded a value of 4.148 Å. We also checked the optPBE-vdW functional for which calculations showed a_0 to be larger: 4.197 Å. All in all, the trend a_0(optPBE-vdW) > a_0(PBE) > a_0(optB86b-vdW) is similar to that reported by Klimeš *et al.* for, e.g., Ag and Cu.[21] To check its performance we performed one calculation using the optPBE-vdW functional to obtain the adsorption parameters of the water monomer on a gold slab modeled by four layers. The results were very similar to those calculated with the optB86b-vdW functional and, therefore, the optPBE-vdW functional was not further used since a_0(optB86b-vdW) is closer to the experimental value.

The geometric adsorption parameters of the water monomer considered here are the distance between the water's O atom and the underlying Au surface atom, $d_{\text{Au-O}}$, and the tilt angle α that describes the angle between the molecular plane of H_2O and the metal surface. The adsorption energy is evaluated using the formula

$$E_{\text{ads}} = (E_{\text{tot}} - E_{\text{Au}} - n \cdot E_{\text{H2O}})/n, \tag{1}$$

where E_{tot} is the energy of the total system, E_{Au} is the energy of the slab alone and E_{H2O} is the energy of one H_2O molecule. n refers to the number of water molecules adsorbed. The molecules are adsorbed on one side of the slab. Here, negative adsorption energies are equivalent to exothermic adsorption.

The MD simulations were performed employing an orthorhombic $c(2\sqrt{3} \times 3)$ super-cell consisting of seven layers, where the middle metal slab layer was kept fixed (Fig. 2). Each layer contains 12 Au atoms. The water layer itself was modeled by 60 H_2O molecules that form a ~19 Å thick solvent layer, resulting in a water density of approximately 1.0 g/cm^3. However, for the PBE functional, the equilibrium of the water density might differ from this value;[47] still, possible artifacts are not expected to occur.[48] Indeed, Poissier *et al.* actually suggested in their article that the PBE functional is a good choice.[15] The proposed temperature for a correct behavior of liquid PBE water is 330 K.[47,48] The reason is that strongly associating liquids are prone to a glassy behavior, and the range of stable liquid densities increases as the temperature is increased away from the triple point.[49] For the sake of consistency, this temperature has been applied with all methodologies used here, independently if the methodology

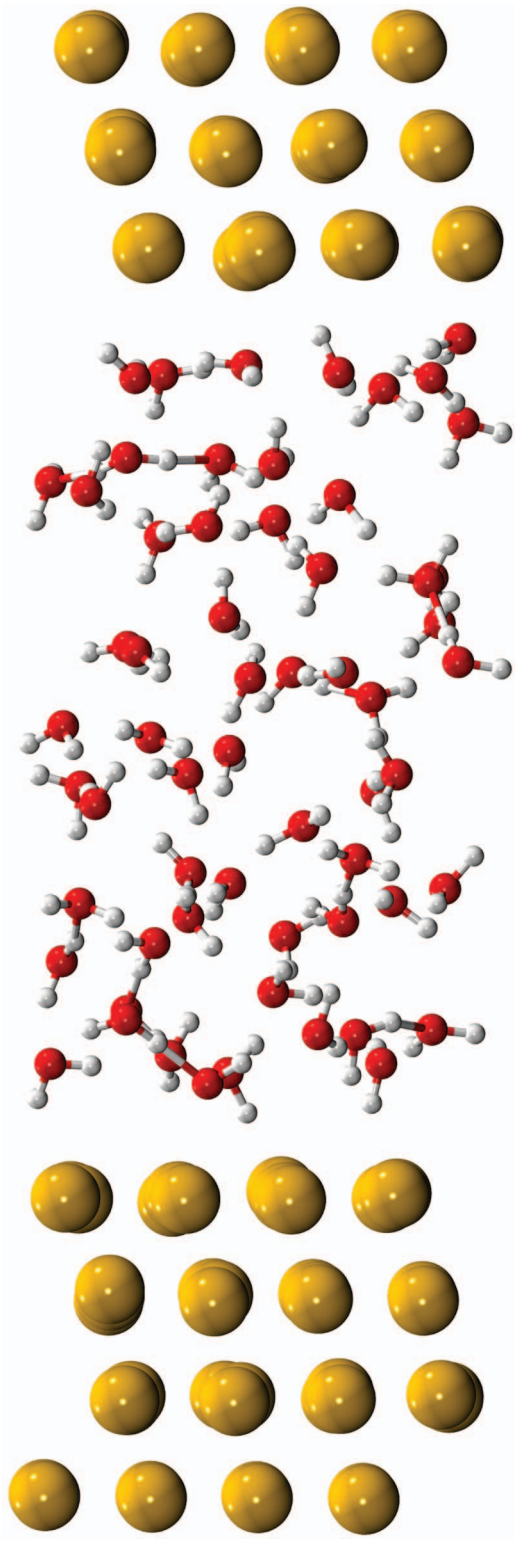

FIG. 2. Snapshot of the Au slab and the H_2O layer as simulated with the optB86b-vdW functional. O atoms are in red, H atoms in white, and Au atoms in yellow.

would represent the liquid state of H_2O at standard conditions well.

To determine the structure of the interface, planar and angular distribution functions were calculated. The planar distribution functions $g(z)$ give the density profile of the solvent in z-direction. Angular distribution functions $p(\varphi, z)$ and $p(\theta, z)$

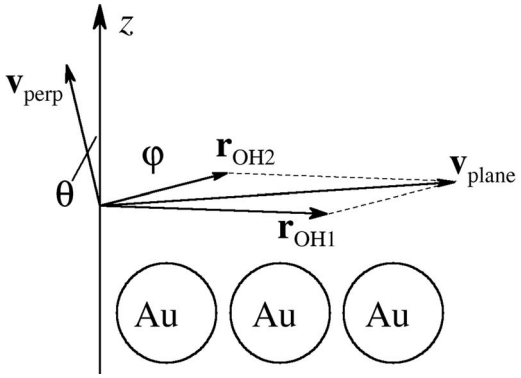

FIG. 3. Sketch of how the angles φ and θ are calculated. The bond vectors $\mathbf{r}_{OH1}$ and $\mathbf{r}_{OH2}$ represent the OH bonds. By taking the sum of these bond vectors, the molecular vector $\mathbf{v}_{plane}$ is obtained, while $\mathbf{v}_{perp}$ is calculated as the vector product. Therefore, $\mathbf{v}_{plane}$ and $\mathbf{v}_{perp}$ are perpendicular to each other. φ and θ are then calculated by including the surface normal z with the vectors $\mathbf{v}_{plane}$ and $\mathbf{v}_{perp}$, respectively.

represent the distribution of the angles φ and θ, depending on the distance from the surface. How these angles are obtained is explained in more detail in Fig. 3. Since $\mathbf{v}_{plane}$ and $\mathbf{v}_{perp}$ are perpendicular to each other, the relation

$$\theta = |90^\circ - (90 - \varphi)| = |\varphi| \quad (2)$$

holds true when both H atoms are at the same height. Additionally, a further relation that helps to interpret these graphs is that when the molecular plane is found to be parallel to the surface normal, then $\theta = 90^\circ$, independently of the orientation of $\mathbf{v}_{plane}$.

Finally, the vibrational spectra reported in this work are obtained by Fourier transforming the normalized velocity autocorrelation function (VACF). Each spectrum was calculated with a correlation time of 2 ps. In order to observe differences in the spectrum between interfacial H_2O molecules and those contained in the bulk water layer, the total water layer was divided into two regions; the two interfaces form one region while the remaining water molecules form the bulk region. Only those atoms that maintain their z-coordinate within the defined limits throughout the correlation time were included to determine the VACF of the interface.

B. Computational details

Density functional calculations were carried out using the VASP code.[50–52] This code solves the Kohn-Sham equations for the valence electron density within a plane wave basis set, and makes use of the projector augmented wave (PAW) method to describe the interaction between the valence electrons and the atomic cores.[53,54] The valence electron density is defined by the $2s^2 2p^4$ electrons of each O atom, the $1s$ electron of the H atom and the eleven valence electrons ($6s^1 5d^{10}$) of each Au atom. The PBE,[55] PBE-D2[17] and the optB86b-vdW[21] functionals were chosen and an energy cutoff of 300 eV was applied to the plane waves for the MD simulations and 500 eV for the three configurations (Au-H_2O, H_2O, Au) needed to calculate the monomeric adsorption parameters. The Gaussian smearing method with $\sigma = 0.2$ eV was used. Structures were optimized using a conjugate-gradient

algorithm until the forces between the ions reached 1.0×10^{-2} eV Å^{-1}. A $3 \times 3 \times 1$ set of **k**-points was used to sample the Brillouin zone for the $p(4 \times 4)$ super-cell model and $5 \times 5 \times 1$ **k**-points for the smaller super-cell with the $p(2 \times 2)$ surface. With this setup the density of the integration mesh is similar for both super-cells. In the MD runs, only the **Γ**-point was employed. The MD simulations were performed in the canonical ensemble at a temperature of 330 K. The temperature was controlled through the Nosé thermostat[56,57] as implemented in VASP, which does not apply velocity rescaling and thus allows calculating VAC functions. The numerical integration was done using a time step set of 0.5 fs.

Before the Au-water system was simulated on a first-principles level of theory, the water layer was equilibrated using a classical force field,[58] using Lennard-Jones parameters for Au as proposed by Heinz *et al.*[59] The slab itself was fixed during the simulation. The parameters of the Au-H_2O interactions were determined by applying the Lorentz-Berthelot mixing rules. These simulations were done using the molecular mechanics driver FIST that is part of the CP2K package.[60] After a 50 ps MD simulation using these force fields in order to obtain a distributed water bulk layer, each system was equilibrated at the first-principles level for 5 ps, followed by a 12 ps production run. Furthermore, a 20 ps MD simulation of 64 H_2O molecules in a cubic box of 12.4 Å, with an applied time step of 0.5 fs in length, was performed. Again, the PBE, PBE-D2, and optB86b-vdW functionals were used to obtain the trajectories.

III. RESULTS

A. Monomeric water adsorption on the Au(1 1 1) surface

With the aim to explore the surface-water interaction and settle a model we start by analyzing the adsorption of a single H_2O molecule on the $p(4 \times 4)$ super-cell surface models with a varying number of slab layers. The thus obtained coverage is equivalent to $\Theta = 1/16$ ML. The results are summarized in Table I. Within a given functional, the adsorption energies are independent on the number of slab layers. Not surprisingly, the PBE adsorption energy is the weakest, with $E_{ads} = -0.11$ eV, therefore reproducing the theoretical results reported earlier,[8–12] while the energies are more exothermic when dispersion interactions are included in the calculation by one way or another. Applying the Grimme semi-empirical dispersion correction it results in −0.24 eV; with the optB86b-vdW functional it is even slightly stronger (−0.30 eV). For the one calculation that was performed using the optPBE-vdW functional, an adsorption energy of −0.27 eV was obtained. Through our calculations we noticed that the dispersion correction adds a consistent part to the adsorption energy, almost tripling the interaction strength between the Au surface and the water monomer obtained with the GGA-only functional.

TABLE I. Slab layer dependent adsorption parameters for a p(4 × 4) super-cell surface. The adsorption energies were found to be −0.11 eV for PBE, −0.24 eV for PBE-D2, and −0.30 eV for the optB86b-vdW functional. α is in degrees, $d_{Au\text{-}O}$ and ΔO_{xy} in [Å].

	PBE			PBE-D2			optB86b-vdW		
n layers	A	$d_{Au\text{-}O}$	ΔO_{xy}	α	$d_{Au\text{-}O}$	ΔO_{xy}	α	$d_{Au\text{-}O}$	ΔO_{xy}
4	4.0	2.77	0.24	−10.3	2.75	0.43	10.5	2.67	0.23
5	5.9	2.80	0.19	−15.1	2.76	0.57	6.9	2.67	0.29
6	8.3	2.77	0.13	−12.7	2.75	0.55	11.4	2.66	0.15
7	−0.8	2.79	0.40	...	...	...	4.9	2.69	0.41
8	8.2	2.77	0.22	...	...	...	12.7	2.66	0.20

Regarding the geometrical parameter, a strict pattern could not been found neither, yet the values do differ for different numbers of n. Starting with the analysis of the adsorption angle α, we find that the results obtained with PBE-D2 are completely unreasonable. For the three systems considered, suspiciously negative adsorption angles are calculated, suggesting that the H atoms have stronger interactions with the Au surface atoms than O atoms. Tonigold and Gross presented adsorption energies of the ice-like water bilayer on different surfaces and found that the H-down structure adsorbs endothermically.[23] Obviously, our finding that H is closer to the surface is counterintuitive. Where the slab is modeled with five Au layers, $\alpha = -15.1^\circ$. It is slightly less negative for the other two slab models. Most certainly, the DFT-D2 methodology does not reproduce well the Au-H_2O interaction because of the fitting of the empirical parameters to an Au-C system and the environment-independent C_6 parameter. It would be interesting to see how the recent DFT-D3 and TS methods describe the adsorption structure of water on a gold surface. Concerning the results obtained with the remaining functionals, it's interesting to note that if the slab is formed with an odd number of layers, the H_2O molecule results to lie flatter on the surface than for the even numbered slabs. For the seven-layered PBE system, α is virtually zero, and for the optB86b-vdW functional the tilt is reduced by about 50% compared to the 6-layered slab.

The gold-oxygen distance, $d_{Au\text{-}O}$, on the other hand is insensitive to the number of slab layers employed. The PBE distance is similar to the PBE-D2 distance, going from ∼2.78 Å (PBE) down to roughly 2.75 Å (PBE-D2). The distance becomes considerably shorter for the optB86b-vdW functional, where $d_{Au\text{-}O}$ drops to 2.67 Å. Cicero *et al.* reported an even shorter PBE-D2 distance (2.54 Å),[11] although whether the screening of the metal was taken into account or not was not reported. Considering the above presented optB86b-vdW bond distances, this value seems to be rather an underestimation of $d_{Au\text{-}O}$. Concerning the horizontal displacement, ΔO_{xy}, we do not observe any dependency on the number of slab layers. However, the oscillations are relatively large, the smallest displacement of the monomer differs by 0.27 Å from the largest ΔO_{xy}.

The dependency of the adsorption geometry and energy of the water monomer on coverage will now be considered. Only results from calculations performed with the PBE and the optB86b-vdW functional are tabulated in Table II. The reported surface models in literature are the $p(2 \times 2)$,[8,9] $p(3 \times 3)$,[10,12] and the $c(3\sqrt{3} \times 5)$[11] super-cell surface. All these models differ in the number of slab layers, in the number of relaxed layers, and the computational set-up. Further details are given in the subscripts and the footnotes in Table II. In the

TABLE II. Adsorption parameters calculated for the atop adsorption site on differently sized Au(1 1 1) surfaces and with different coverage. The computational details for calculations reported earlier in literature are summarized in the footnotes. Coverage is given in [ML], E_{ads} in [eV], the tilt angle α in degrees, ΔO_{xy} and $d_{Au\text{-}O}$ in [Å]. The subscript in Θ indicates the size of the super-cell surface.

	PBE				optB86b-vdW			
Coverage	E_{ads}	α	$d_{Au\text{-}O}$	ΔO_{xy}	E_{ads}	α	$d_{Au\text{-}O}$	ΔO_{xy}
$\Theta_{2\times2\times7} = 1/4$	−0.11	−3.6	2.94	0.15	−0.29	−0.4	2.76	0.23
$\Theta_{4\times4\times7} = 1/4$	−0.11	−5.6	2.92	0.28	−0.29	−2.5	2.76	0.30
$\Theta_{4\times4\times7} = 1/8$	−0.12	3.8	2.85	0.20	−0.30	9.6	2.72	0.11
$\Theta_{4\times4\times7} = 1/16$	−0.11	−0.8	2.79	0.40	−0.30	4.9	2.69	0.41
$\Theta_{2\times2\times5,6} = 1/4$[a]	−0.13	13	3.02	0.06	…	…	…	…
$\Theta_{2\times2\times3} = 1/4$[b]	−0.17	flat	…	…	…	…	…	…
$\Theta_{3\times3\times3} = 1/9$[c]	−0.14	10	2.63	0.06	…	…	…	…
$\Theta_{3\sqrt{3}\times5\times4} = 1/12$[d]	−0.12	5	2.81	…	…	…	…	…
$\Theta_{3\times3\times7} = 1/9$[e]	−0.11	6	2.67	…	…	…	…	…

[a] Values taken from Ref. 8. PW91 with US-PP. 5 or 6 layers were used to model the slab.
[b] Values taken from Ref. 9. PW91 with US-PP. Au slab was kept frozen entirely.
[c] Values taken from Ref. 10. PW91 with US-PP. Top layer was allowed to relax.
[d] Values taken from Ref. 11. PBE with US-PP. Au slab was relaxed entirely.
[e] Values taken from Ref. 12. PW91 with US-PP. Top layer was allowed to relax.

present study, we investigate coverage ranging from $\Theta = 1/16$ to 1/4 ML using the $p(2 \times 2)$ and $p(4 \times 4)$ super-cell model surfaces. Coverage of $\Theta = 1/8$ and 1/4 ML was obtained by adsorbing either 2 or 4 water molecules on the surface as indicated in Fig. 1.

As can be observed in Table II, the adsorption energy remains practically unchanged for the coverage considered here and equals the corresponding energies mentioned above. Still, a tiny lowering of the adsorption energy can be observed for both functionals considered when the coverage is larger than 1/8 ML, the change, however, is smaller than 1%. In general, the results in Table II are comparable to those presented in other reports[8–12] in the sense that H_2O adsorbs parallel to the slab surface and that the surface-water interaction is weak. Concerning the results we present here we find that the Au-O distance, $d_{Au\text{-}O}$, increases each time H_2O molecules are added to the surface, as it could be expected. In the PBE case it increases by 0.15 Å from 2.79 if $\Theta = 1/16$ ML to 2.92 and 2.94 Å, respectively, depending on the slab model. When dispersion forces are included the difference is only 0.07 Å, a small differentiation but it is still perceivable. Then, both computational approaches give the same pattern for the tilt angle α. It decreases in the order $\Theta_{4\times4\times7} = 1/8$ ML $> \Theta_{4\times4\times7} = 1/16$ ML $> \Theta_{2\times2\times7} = 1/4$ ML $> \Theta_{4\times4\times7} = 1/4$ ML. Strangely, the angles become negative when the coverage is larger and, when the surface is modeled with the larger super-cell, the results display even greater negative angles. Such a result was not anticipated as it contradicts any of the theoretical studies of the water monomer adsorbed on the Au(1 1 1) surface. We therefore performed a set of single point calculations where the angle α and the distance $d_{Au\text{-}O}$ were varied systematically. The results are plotted in Fig. 4. The largest differences in E_{ads} are at most 27 meV. Between the smallest positive tilt angle ($\alpha = 5°$) and the optimum one a difference of only 3 meV is calculated. Yet, it is still the above reported optimized adsorption geometry that is the most stable one, however, the differences are very small. In Figs. 5 and 6 the charge density $\Delta\rho$ is represented, which was obtained as $\Delta\rho = \rho_{total} - \rho_{surface} - \rho_{H2O}$. They were obtained using the optB86b-vdW functional. The isosurfaces represented in Fig. 5(a) are similar to those reported by Michaelides *et al.*[8] However, there are some differences. On the Au surface atoms that are closest to the H atoms, one finds an increased amount of charge density. In Fig. 6(a) the increase occurs on all Au atoms that surround the surface atom on which water is adsorbed. This explains nicely why H_2O can be adsorbed

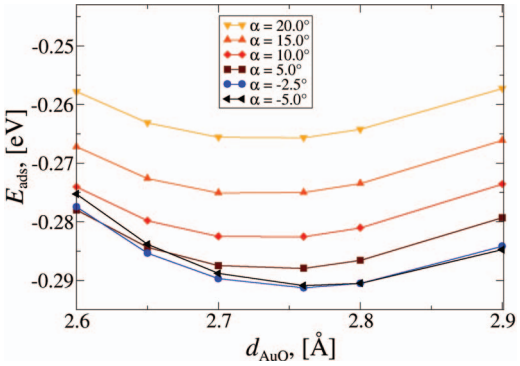

FIG. 4. Adsorption energies in function of the Au-O distance. Each line represents a different tilt angle. The lines for $\alpha = -5.0°$ and $-2.5°$ do nearly coincide. The largest ΔE_{ads} is about 27 meV, while it differs by roughly only 3 meV when $\alpha = -2.5°$ and 5.0° are compared at a distance of 2.76 Å.

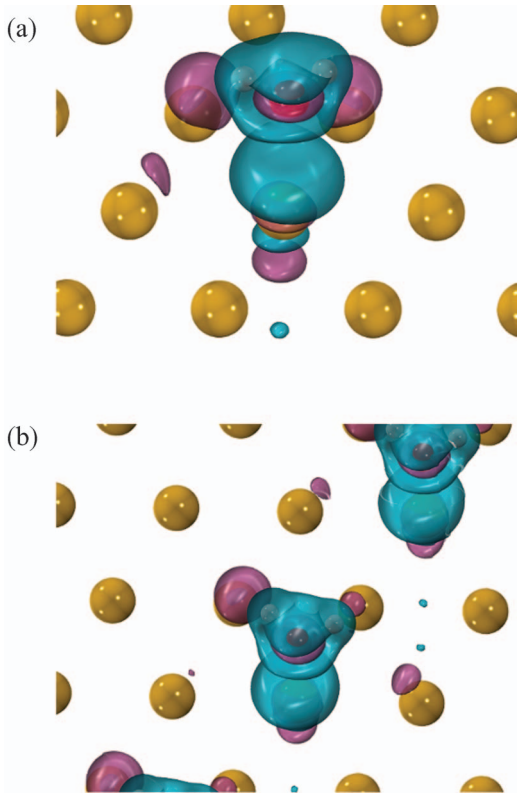

FIG. 5. Charge density difference plots of H_2O adsorbed on the $p(4 \times 4)$ super-cell surface model for the optB86b-vdW functional. Mauve color indicates gain, cyan color loss of charge density. Coverage is $\Theta = 1/16$ ML in (a), and 1/8 ML in (b). An isovalue of $\pm 2.0 \times 10^{-4}$ e/Bohr^3 has been applied to display the isosurfaces. O atoms are in red, H atoms in white, and Au atoms in yellow.

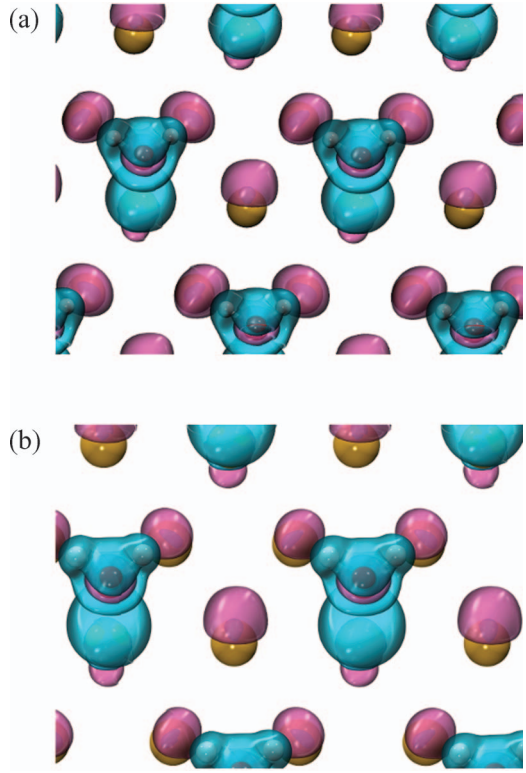

FIG. 6. The same illustration as in Fig. 5 but for the highest coverage considered here ($\Theta = 1/4$ ML). In (a) the charge density difference plot is given for the optimized system, while in (b) the tilt angle has been set to 20.0°. The adsorption distance is the same as in (a).

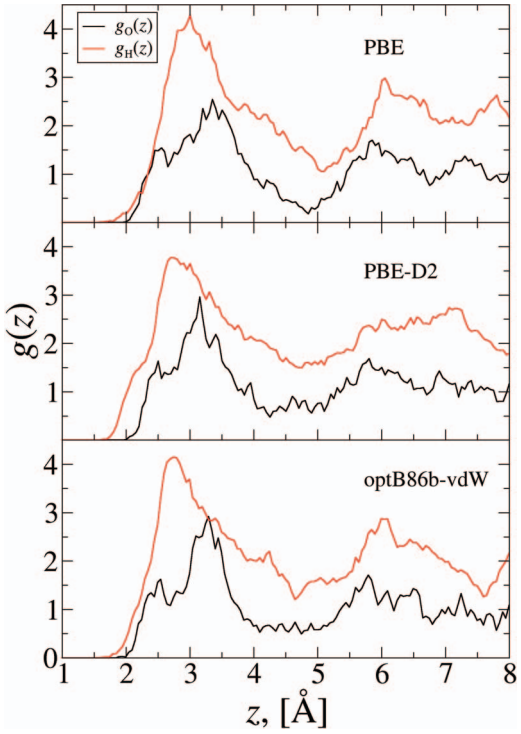

FIG. 7. Planar distribution functions $g(z)$ of O (black line) and H (red line) for the three systems. The functions are normalized to the bulk water density. The bin size is set to 0.05 Å.

with negative tilt angles on Au(1 1 1) when the coverage is relatively high. To rule out the possibility that the stronger polarization of the Au surface might be induced accidentally by the H atoms during the geometry optimization, the same plot is represented in Fig. 6(b) for an H_2O molecule that is adsorbed at the optimized Au-O distance but with a tilt angle of 20°. As can be seen these $\Delta\rho$ plots are nearly identical. Therefore, small, negative tilt angles are reasonable. In Fig. 5(b) the charge density increase is not symmetric with respect to the mirror plane in H_2O and, as a consequence, the H atoms are not at the same height. Again, similar to Poissier *et al.*,[15] we find that it is important to employ a large enough surface model in order to ensure that the properties of the H_2O monomer are represented correctly.

B. MD simulations of the Au(1 1 1)-H_2O interface

In this section the MD simulations will be analyzed, the main focus lying on the structure of H_2O in the Au-water interface. First, the planar distribution graphs $g(z)$ represented in Fig. 7 together with the corresponding $p(\varphi, z)$ and $p(\theta, z)$ probability distribution functions in Fig. 8 will be examined. The $g(z)$ functions are normalized to the liquid water density of 1.0 g/cm^3, therefore, the peaks in the $g_H(z)$ function are higher than those in the $g_O(z)$. The origin is defined as the mean z-value of the outermost Au layer. In Table III the maxima of the peaks have been tabulated as they were extracted from Fig. 7. Within the same table there are also the approximate values for the angles φ and θ listed which define the orientation of the molecular vectors' $\mathbf{v}_{plane}$ and $\mathbf{v}_{perp}$, respectively. We emphasize on two or three areas, depending on the functional applied, that are visible in the probability distribution plots of the angle φ. They are recognized as blue areas, where the highest number of molecules with a given angle is counted, and they are denoted as *A*, *B*, and *C*. In $p(\theta, z)$ only two areas are introduced, labeled *S* and *T*.

We start the analysis with the structure of H_2O within the interface which is basically found within all systems but with differing probabilities as will be discussed in the following part. To this end we will first discuss the results obtained with the optB86b-vdW functional. From the $g_O(z)$ function represented in the lowest panel in Fig. 7 (black line) we can estimate that the interface extends between 2 and 4 Å away from the Au surface and is divided in two sub-layers where at most three different orientations can be determined, corresponding to the areas *A*, *B*, and *C* in Fig. 8(a). We can therefore support the interpretation of the broad first experimental peak obtained in x-ray experiments[33] made by Halley *et al.*[61] They presume that this peak is not just one broad peak, but rather it is composed by two, experimentally unresolved peaks. We clearly see in the panel corresponding to the optB86b-vdW functional in Fig. 7 that one nearer sub-layer, sub_{near}, has been formed with its maximum at roughly 2.4−2.6 Å and a second, more intense sub-layer, sub_{far}, is located between 3.2 and 3.4 Å. The Au-O distances obtained with the PBE functional are 0.1 Å larger than those obtained with the optB86b-vdW and PBE-D2 functionals.

We still focus on the optB86b-vdW $g_O(z)$ and $g_H(z)$ functions represented in the lowest panel in Fig. 7 (black and red lines, respectively) and recognize the two sub-layers

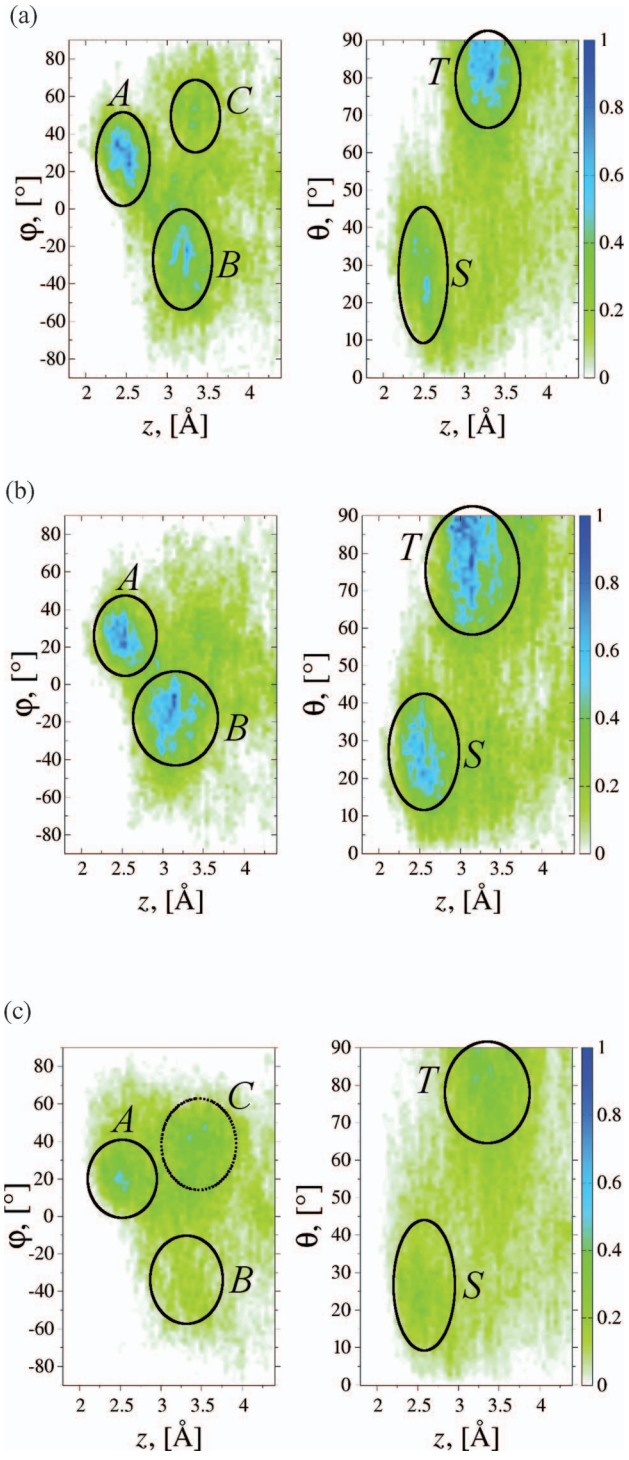

FIG. 8. Angle distribution functions $p(\varphi, z)$ and $p(\theta, z)$. In (a) the plots for the optB86b-vdW are given, in (b) for PBE-D2 and in (c) for the PBE functional. The circles *A*, *B*, and *C* correspond to the areas as they are discussed in the text. The corresponding values are tabulated in Table III. The center of mass is used to determine the position in z. The bin size for z is 0.05 Å, and 2.0 and 1.0° for φ and θ, respectively.

mentioned above. The complete first adsorption layer does extend over 2.9 Å. By integrating the unnormalized $g_O(z)$ function (not represented here) over this range we obtain a molecular density of 1.08 g/cm^3. Obviously, the increase is smaller than 10%, far from the 200% increase reported by Toney *et al.*[33] Such a large discrepancy has led us to agree

TABLE III. Au-O distances and angles φ and θ as obtained via $g_O(z)$, $p(\varphi, z)$ and $p(\theta, z)$. For each angle, the center of the range is given with the approximate limits in parenthesis. $d_{Au\text{-}O}$ is given in [Å], φ and θ in degrees.

Functional	Area	$d_{Au\text{-}O}$	φ	Θ
PBE	*A*	2.6	20 (±15)	25 (±10)
	B	3.4	−40 (±20)	80 (±10)
	C	3.4	30 (±30)	80 (±10)
PBE-D2	*A*	2.5	25 (±15)	25 (±15)
	B	3.2	−15 (±15)	80 (±10)
optB86b-vdW	*A*	2.5	30 (±10)	25 (±15)
	B	3.3	−25 (±15)	80 (±10)
	C	3.3	50 (±20)	80 (±10)

with other studies that, too, have questioned the massive density increase.[36–38]

Coming back to the analysis of the optB86b-vdW interfacial structure we see that in the sub-layer sub_{near} the number of O atoms $n_O \approx 1.5$. This sub-layer has been reported by Cicero *et al.* too using the PBE-D2 methodology, although they found that only a shoulder forms at this position.[11] From the $g_H(z)$ function we observe that the peak reaches about 4 H atoms per unit area. Since this is more than twice the number of O atoms, one can speculate that here H_2O is adsorbed O-down, attributing the one remaining H atom to molecules located further away from the surface. To obtain the actual orientation of the involved water molecules we have to analyze the angular probability plots in Fig. 8(a). From Table III we find in area *A* the tilt angle φ to be centered at 30° and the corresponding angle θ in area *S* is about 25°. Since θ is similar to φ, one can apply Eq. (2) and finds that here the H atoms must have roughly the same z-coordinate. Therefore, interfacial H_2O in sub_{near} is oriented O-down.

Next, the sub-layer sub_{far} located at 3.3 Å is analyzed. From Table III it can be immediately seen that the molecular plane is parallel to the z-axis since $\mathbf{v}_{perp}$ in area *T* is roughly perpendicular to the surface normal ($\theta \approx 85°$). In area *B* the angle φ is negative which results in the vector $\mathbf{v}_{plane}$ pointing more towards the slab surface. Because φ and θ do not have the same magnitude, the H atoms are at different heights with respect to the distance from the slab surface. Therefore, we may subtract 52.5°, which corresponds to one half of the bond angle α_{HOH}, from φ and obtain the tilt angle of the one OH bond that points to the slab. It results in it being around 80°, indicating that this bond is almost perpendicular to the Au surface. There is a third area *C* which is only weakly observed. φ is found to be 50°, $\theta \approx 80°$. This results in a second orientation of H_2O within sub_{far} where one OH bond is parallel to the surface and the other is oriented towards the bulk water layer although not perpendicular. On metallic surfaces, two models were assumed to exist. These models described the ice-like bilayer structure, the H-up and the H-down model. We use these models simply to depict the observed structures presented herein with a widely known model because it serves quite well for this task. By no means do we want to discuss the model itself, since it was shown that it does not represent well enough the many different structures of water on different metal surfaces.[4–7] The

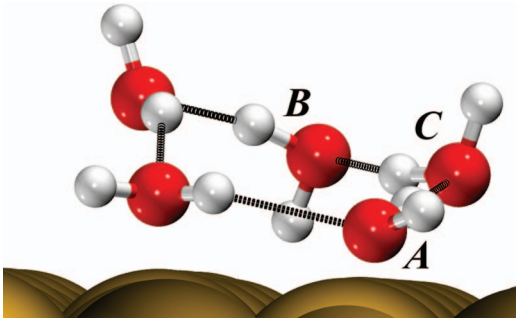

FIG. 9. Side view of a snapshot taken from the MD simulation performed with the optB86b-vdW functional. The remaining molecules that form the water layer are not included for reasons of visibility. *A*, *B*, and *C* refer to the orientations as they are derived from the corresponding areas in Fig. 8 and Table III. Molecule *B* is an example of the simplified H-down orientation of an ice layer above a metal surface, molecule *C* represents the H-up model. In black are the hydrogen bonds drawn. O atoms are in red, H atoms in white, and Au atoms in yellow.

combinations *A*/*B* and *A*/*C* do coincide with those models and by comparing the probabilities of finding these combinations, one can conclude that both orientations do coexist, but the combination *A*/*B* is the preferred and, therefore, the more stable one. In Fig. 9 a snapshot from the optB86b-vdW trajectory is represented where molecules with orientation *A*, *B*, and *C* are indicated. In this figure the molecules form a pentameric ring structure. Apart from the pentamer we also found tetra-, hexa- and heptameric ring structures. The analysis was performed by eye only. A few figures of snapshots that represent typical ring structures throughout the trajectory are added to the supplementary material.[62] In these figures the atoms are colored depending on their z-coordinate in order to recognize their relative arrangement. So, within a condensed water layer above the Au(1 1 1) surface, we found similar structures as were reported in the work of Nie *et al.*[5] They found, for the first wetting layer of H_2O on a Pt(1 1 1) surface, that penta- and heptameric structures coexist with six-membered rings. In the present case the coexistence is less obvious since all kinds of coexisting structures can be observed. Indeed, there are short moments where tetra-, penta-, hexa- and heptamers can be observed at once, although some of the rings are heavily distorted (see Fig. S1 in the supplementary material).[62] It is worth noting that these ring structures usually form over both sublayers and that they are rarely formed planarly on the surface. Furthermore, they are usually quite distorted. The most stable combinations we could observe are a hexamer with another hexameric ring (Fig. S2 in the supplementary material),[62] and pentamers together with hexa- and heptamers (Figs. S3 and S4 in the supplementary material).[62] Tetramers also form next to all of the aforementioned ring structures but only for a relatively short period of time (Figs. S5 and S6 in the supplementary material).[62]

We now compare the interfacial structure obtained with the optB86b-vdW functional with those obtained using the PBE functional and its dispersion corrected PBE-D2 variation. For the latter, we can see in the middle panel of Fig. 7 that the $g(z)$ functions are reproduced quite similarly to the optB86b-vdW $g(z)$ functions. Also, the angular probability functions represented in Fig. 8(b) for both functionals resemble each other except that area *C* is not as developed as in Fig. 8(a). Additionally, the areas differ in their blue intensity but the differences are rather small. Therefore, the general picture of the interfacial structure is the same.

We finish this part by looking at the results obtained via the PBE functional. The corresponding $g(z)$ functions are plotted in the upper panel of Fig. 7. We see that they are also reproduced very similarly to those for the optB86b-vdW functional, but in Fig. 8(c) we observe that the probability is distributed very flatly over the plotted range. The space between the highlighted areas is almost uniformly colored in green. Only in the areas *A*, *C*, and *T* do some blue spots indicate a slightly higher probability for finding φ or θ at these z-coordinates. Finally, the area *B* is marked only to show that $p(\varphi, z)$ is very small there.

Concluding this analysis of the interfacial structure of H_2O, we find that the molecules in the sub_{near} sub-layer are oriented O-down, whereas two species of H_2O molecules are found in sub_{far}. One species has one OH bond pointing nearly perpendicular to the surface, with the molecular plane parallel to the z-axis. The other one has one OH bond oriented away from the Au surface, while the second bond is parallel to it. Most certainly there are H-bonds formed between H_2O in sub_{near} and sub_{far}. Furthermore, one can hypothesize that the molecules closer to the surface are better H-bond acceptors than donors since the molecular orientation in area *B* is more probable to occur than in area *C*. This indeed is the interfacial structure as it was reported earlier for this specific system.[11]

Although weaker, the strength of the H_2O-Au interaction is comparable to the strength of a typical H-bond. The orientation of H_2O closest to the surface indicates that such a weak bond between the gold surface atoms and the H_2O molecule occurs, where H_2O acts as a bond acceptor and the Au surface atoms as donors. Consequently, these water molecules will then themselves be able to donate 2 H-bonds and accept 1 hydrogen bond to/from the next layer of H_2O. This can be seen, for example, in Fig. 9 where molecule *A* accepts and receives 1 H-bond each. The second donated H-bond is not represented in this figure. Therefore, for H_2O in sub_{near} a maximal number of hydrogen bonds has to be expected that is roughly 1 unit smaller than the typical number of 3.6 H-bonds per H_2O molecule, which actually can be observed in Fig. 10 for the three methodologies. As pointed out by Cicero *et al.*, the number of donating hydrogen bonds is slightly higher or equal than the average number of donated H-bonds in liquid water.[11] Therefore, the H_2O molecules in the gold-water interface form stronger H-bonds than in the liquid water layer between the gold surfaces.

The hydrogen-bond-strength itself can be estimated by comparing the vibrational spectra of a pure water system and the system of interest, here being Au-H_2O. The corresponding graphs are represented in Fig. 11 and the values extracted from them are tabulated in Table IV. The frequencies, as they were extracted from these plots, are tabulated in Table IV. Three major features are observed: the librational modes band, ν_{lib}, between 300 and 1100 cm^{-1}, the bending modes, ν_{bend}, with the corresponding peak at $\sim$1600 cm^{-1}, and a strong and broad band for the symmetric and

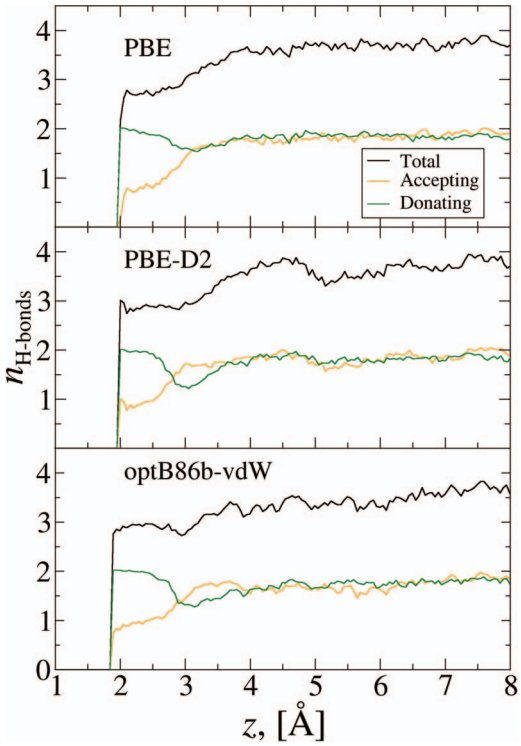

FIG. 10. Functions of the H-bonds for the three methodologies employed. Black line refers to the total number of H-bonds, orange to the number of bond acceptors, and green to the number of donors. The H-bonds are defined as such that $d_{\text{O-O}} \leq 3.5$ Å and the bond angles $\alpha_{\text{OH-O}} \leq 140^{\circ}$.

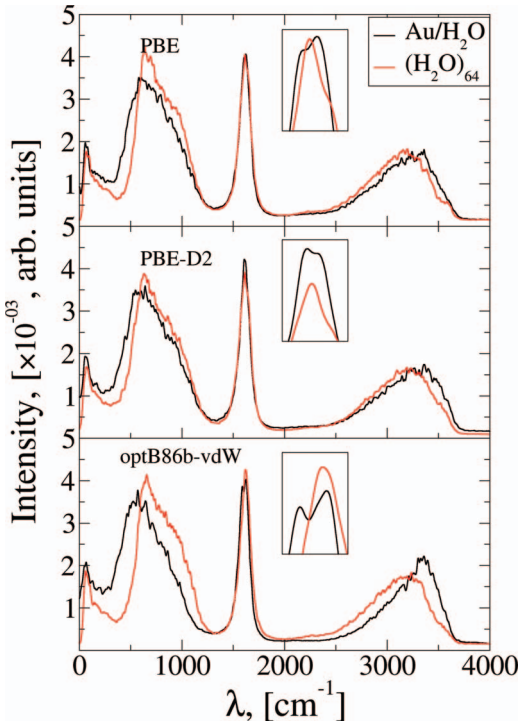

FIG. 11. Vibrational spectra of Au-H_2O and pure H_2O for PBE, PBE-D2 and optB86b-vdW, starting with the top panel. The spectra for the Au-H_2O systems are represented by black lines, the pure water systems by red lines. The inset in each graph represents the peak for ν_{bend} in order to show the splitting of this band when H_2O interacts with the Au surface. The scale of the intensity axis is the same in all graphs.

TABLE IV. Position of the librational, bending, and stretching modes as obtained from Figs. 11 and 12. For the librational and stretching modes the maxima are given, while two peaks for ν_{bend} are tabulated due to metal-water interactions, where available. See main text for details. All numbers are given in [cm^{-1}].

Functional	System	ν_{lib}	ν_{bend}	ν_{stretch}
PBE	$Au_{84}(H_2O)_{60}$	603	1605, 1622	3310
	Interface	495	1598, 1629	3314
	$(H_2O)_{64}$	636	1614	3175
PBE-D2	$Au_{84}(H_2O)_{60}$	602	1607, 1618	3310
	Interface	555	1604	3350
	$(H_2O)_{64}$	630	1611	3210
optB86b-vdW	$Au_{84}(H_2O)_{60}$	568	1588, 1624	3350
	Interface	492	1565, 1587	3350
	$(H_2O)_{64}$	656	1620	3180

asymmetric stretching modes, ν_{stretch}, centered between 3100 and 3700 cm^{-1}. As can be observed, the presence of a gold surface does have an influence, independently on the applied methodology. The bending mode ν_{bend}, for instance, splits up upon inclusion of the gold slab, indicating that the surface influences the bond angles of water. This effect can be best observed in the insets in Fig. 11. This is true for all cases, however, the effect is mostly pronounced when the dispersion forces are included with the optB86b-vdW functional. Here, the second peak that has formed is located at lower wave numbers, an indicator for larger bond angles. For the PBE functional, with and without semi-empirical dispersion correction, the splitting occurs too, but the center of the band remains at the same position. Furthermore, for all systems the librational mode bands redshift, and the stretching mode bands blueshift. A similar observation was reported by Zelsman, and Lock and Bakker.[63,64] However, the investigated parameter in their experimental reports was the temperature rather than a metal surface. They found that the librational mode bands and the stretching mode bands shift to the red and blue, respectively, upon raising the temperature. This occurs when the H-bonds become weaker, and, as a consequence, the rocking movement of the H_2O molecules is achieved more easily (redshift of librational modes) and the OH bonds get stronger and shorter (blueshift of the stretching modes). From this analysis, we can draw the conclusion that the H-bond network is actually weakened by the Au slab surface. This is supported also by Li *et al.* by showing that when the redshift of, in their case, the stretching mode becomes larger, the H-bond becomes stronger.[65] Yet, it has been reported that the hydrogen bond strength also decreases when the pressure increases.[66–68]

In the present setup one might think that the observed shifts could be induced by an expansion of the slab in the direction of the surface normal. Over the course of the simulation the surface atoms most certainly do expand and contract. If one observes the trajectory he will see that the surface Au atoms do move vertically, so it would be reasonable to think that the pressure on the water layer is not constant. To show that this is not the reason for the observed differences we divided the water layer in two parts. The two interfacial regions were put together to form one part and the remaining bulk water molecules formed the second. For both parts

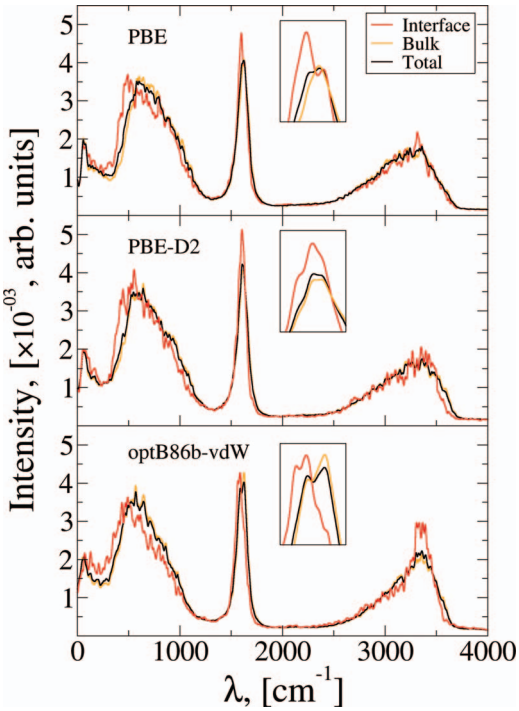

FIG. 12. The same vibrational spectra as in Fig. 11, but here the total water layer (black line) was divided into a bulk part (orange line) and an interfacial part (red line). The graphs from the interfacial parts differ from the remaining spectra indicating that it actually is the Au-H_2O interaction that weakens the H-bond network of the water layer.

the vibrational spectra were calculated and plotted in Fig. 12. The spectra of the total water layer (black lines) are very similar, although not equal, to the spectra obtained from the bulk-only part (orange lines). The differences show up in the spectra calculated for the interfacial part (red lines), most obviously observed for the librational modes. These are clearly shifted to the red for all systems investigated. The stretching mode bands virtually do not shift, but the resulting intensities are higher, especially for the optB86b-vdW functional. Also, the bending modes are quite sensitive to the Au-H_2O interactions. As mentioned above, the band peak of this mode is more or less split, depending on the applied methodology. Clearly, these spectra show that it is indeed the interaction between surface Au atoms and H_2O which changes the properties of the water hydrogen bond network of the system and, as a result, the corresponding spectrum. Therefore, taking into account that we found that the molecules in the two sub-layers do form H-bonds, we can state that the Au(1 1 1) surface at the *pzc* indeed does weaken the H-bond network but not so strongly as to disrupt it.

If we compare the peak positions for the $Au_{84}(H_2O)_{60}$ systems in Table IV we see that where the dispersion corrected PBE-D2 and the original PBE functional are employed, the extracted peaks are located at very similar wave numbers while ν_{lib} and $\nu_{stretch}$ obtained with the optB86b-vdW functional are shifted to the red and the blue, respectively, by around 40 cm^{-1}. Thus, it is crucial to include the dispersion forces in an accurate manner and it would be interesting to see how the most recent semi-empirical methodologies, such as the Grimme DFT-D3 and the TS approaches, would perform compared to the optB86b-vdW functional.

IV. CONCLUSIONS

In this report we present the theoretical investigation of the Au-H_2O interface, based on PBE, PBE-D2, and optB86b-vdW geometry optimizations and MD simulations. Investigating the isolated water molecule adsorption on the Au(1 1 1) surface revealed that the weak vdW interaction contributes significantly to the adsorption energy of H_2O on the Au surface, nearly tripling the interaction energy when the PBE and the optB86b-vdW energies are compared. The PBE-D2 results for the monomeric water adsorption gave rather unreasonable results even though screening effects were accounted for by applying the R and C_6 terms only on the surface atoms. Results for the tilt angle were clearly negative, while $d_{Au\text{-}O}$ was similar to the PBE distance. All in all, the typical adsorption structure of a water monomer above an Au surface was obtained, which is the O-down orientation with a tilt angle being nearly parallel to the surface. The effect of coverage is found to be more important. With increasing coverage the Au-O distance increased as well, the effect being more pronounced for the PBE functional. Also, when coverage is set to 1/4 ML, the tilt angle α was shown to be slightly negative when the optB86b-vdW functional was used. Obviously, to correctly describe the monomeric case of water adsorption the chosen slab surface model has to be large enough. The slab thickness is not found to be a determining technical detail. Yet it was found that the tilt angle on odd numbered slabs is slightly smaller than on even numbered ones.

The MD simulations show that optB86b-vdW and PBE-D2 calculations lead to a water layer that is 0.1 Å closer to the Au surface than the PBE distance. Still, this increase in interactional strength does not go along with a massive density increase in the first adsorption layer. Contrary to the x-ray results reported by Toney *et al.*,[33] we obtain only a slight density increase of 8%. Within the first adsorption layer of H_2O on Au(1 1 1), two main orientations are determined. In the sub-layer sub_{near} H_2O is adsorbed O-down, whereas further away in sub_{far} it is oriented as such that one OH bond points to the surface, nearly perpendicular, and the molecular plane is parallel to the z-axis. A third orientation was found from the optB86b-vdW simulation where the molecular plane is also parallel to the surface normal, but the OH bond closer to the slab is oriented parallel to the surface. In general, these orientations are observed for all methodologies investigated. During the simulation, several ring structures were observed, ranging from tetra- up to heptamers.

Finally, we found that the inclusion of an Au(1 1 1) slab does change the strength of the H-bond network, independently of the theoretical approach applied. Comparable to the effect when the temperature is increased, the H-bonds become weaker and the OH bonds stronger, which is manifested by the redshift of the librational modes and the blueshift of the stretching mode bands. Furthermore, a splitting of the bending mode is observed, and for the optB86b-vdW functional a redshift of this band is observed. Using this functional the ν_{lib}

and ν_{stretch} bands are shifted by 40 cm^{-1} to the red and the blue, respectively.

ACKNOWLEDGMENTS

This work was funded by the Spanish Ministerio de Ciencia e Innovación, MICINN, Project Nos. MAT2012-31526 and CSD2008-0023. R.N. thanks the Junta de Andalucía for a predoctoral grant (P08-FQM-3661). Part of the calculations has been carried out at the Barcelona Supercomputing- Center Centro Nacional de Supercomputación (Spain).

[1] A. Hodgson and S. Haq, Surf. Sci. Rep. **64**, 381 (2009).
[2] M. Henderson, Surf. Sci. Rep. **46**, 1 (2002).
[3] P. Thiel and T. Madey, Surf. Sci. Rep. **7**, 211 (1987).
[4] J. Cerdá, A. Michaelides, M.-L. Bocquet, P. J. Feibelman, T. Mitsui, M. Rose, E. Fomin, and M. Salmeron, Phys. Rev. Lett. **93**, 116101 (2004).
[5] S. Nie, P. J. Feibelman, N. C. Bartelt, and K. Thürmer, Phys. Rev. Lett. **105**, 026102 (2010).
[6] J. Carrasco, A. Michaelides, M. Forster, S. Haq, R. Raval, and A. Hodgson, Nature Mater. **8**, 427 (2009).
[7] J. Carrasco, A. Hodgson, and A. Michaelides, Nature Mater. **11**, 667 (2012).
[8] A. Michaelides, V. A. Ranea, P. L. de Andres, and D. A. King, Phys. Rev. Lett. **90**, 216102 (2003).
[9] S. Kandoi, A. A. Gokhale, L. C. Grabow, J. A. Dumesic, and M. Mavrikakis, Catal. Lett. **93**, 93 (2004).
[10] A. A. Phatak, W. N. Delgass, F. H. Ribeiro, and W. F. Schneider, J. Phys. Chem. C **113**, 7269 (2009).
[11] G. Cicero, A. Calzolari, S. Corni, and A. Catellani, J. Phys. Chem. Lett. **2**, 2582 (2011).
[12] S. Meng, E. G. Wang, and S. Gao, Phys. Rev. B **69**, 195404 (2004).
[13] P. J. Feibelman, Science **295**, 99 (2002).
[14] P. Vassilev, R. van Santen, and M. Koper, J. Chem. Phys. **122**, 054701 (2005).
[15] A. Poissier, S. Ganeshan, and M.-V. Fernández-Serra, Phys. Chem. Chem. Phys. **13**, 3375 (2011).
[16] R. Nadler and J. F. Sanz, J. Mol. Model **18**, 2433 (2011).
[17] S. Grimme, J. Comput. Chem. **27**, 1787 (2006).
[18] S. Grimme, J. Antony, S. Ehrlich, and H. Krieg, J. Chem. Phys. **132**, 154104 (2010).
[19] A. Tkatchenko and M. Scheffler, Phys. Rev. Lett. **102**, 073005 (2009).
[20] M. Dion, H. Rydberg, E. Schröder, D. C. Langreth, and B. I. Lundqvist, Phys. Rev. Lett. **92**, 246401 (2004).
[21] J. Klimeš, D. R. Bowler, and A. Michaelides, Phys. Rev. B **83**, 195131 (2011).
[22] B. Hammer, L. B. Hansen, and J. K. Nørskov, Phys. Rev. B **59**, 7413 (1999).
[23] K. Tonigold and A. Gross, J. Comput. Chem. **33**, 695 (2012).
[24] Y. Xue, J. Chem. Phys. **136**, 024702 (2012).
[25] K. Lee, É. D. Murray, L. Kong, B. I. Lundqvist, and D. C. Langreth, Phys. Rev. B **82**, 081101(R) (2010).
[26] S. D. Chakarova-Käck, E. Schröder, B. I. Lundqvist, and D. C. Langreth, Phys. Rev. Lett. **96**, 146107 (2006).
[27] E. Ziambaras, J. Kleis, E. Schröder, and P. Hyldgaard, Phys. Rev. B **76**, 155425 (2007).
[28] J. Klimeš, D. R Bowler, and A. Michaelides, J. Phys.: Condens. Matter **22**, 022201 (2010).
[29] I. Hamada, K. Lee, and Y. Morikawa, Phys. Rev. B **81**, 115452 (2010).
[30] J. Carrasco, B. Santra, J. Klimeš, and A. Michaelides, Phys. Rev. Lett. **106**, 026101 (2011).
[31] M. J. McGrath, I.-F. W. Kuo, and J. I. Siepman, Phys. Chem. Chem. Phys. **13**, 19943 (2011).
[32] J. Wang, G. Román-Pérez, J. M. Soler, E. Artacho, and M.-V. Fernández-Serra, J. Chem. Phys. **134**, 024516 (2011).
[33] M. Toney, J. Howard, J. Richer, G. Borges, J. Gordon, O. Melroy, D. Wiesler, D. Yee, and L. Sorensen, Nature (London) **368**, 444 (1994).
[34] K. Ataka, T. Yotsuyanagi, and M. Osawa, J. Phys. Chem. **100**, 10664 (1996).
[35] M. Ito, Surf. Sci. Rep. **63**, 329 (2008).
[36] I.-C. Yeh and M. L. Berkowitz, Chem. Phys. Lett. **301**, 81 (1999).
[37] P. S. Crozier, R. L. Rowley, and D. Henderson, J. Chem. Phys. **113**, 9202 (2000).
[38] A. Roudgar and A. Gross, Chem. Phys. Lett. **409**, 157 (2005).
[39] S. Schnur and A. Gross, New J. Phys. **11**, 125003 (2009).
[40] I-C. Lin, A. P. Seitsonen, M. D. Coutinho-Neto, I. Tavernelli, and U. Rothlisberger, J. Phys. Chem. B **113**, 1127 (2009).
[41] R. W. Williams and D. Malhotra, Chem. Phys. **327**, 54 (2006).
[42] M.-T. Nguyen, C. A. Pignedoli, M. Treier, R. Fasel, and D. Passerone, Phys. Chem. Chem. Phys. **12**, 992 (2010).
[43] K. Tonigold and A. Gross, J. Chem. Phys. **132**, 224701 (2010).
[44] E. R. McNellis, J. Meyer, and K. Reuter, Phys. Rev. B **80**, 205414 (2009).
[45] G. Mercurio, E. R. McNellis, I. Martin, S. Hagen, F. Leyssner, S. Soubatch, J. Meyer, M. Wolf, P. Tegeder, F. S. Tautz1, and K. Reuter, Phys. Rev. Lett. **104**, 036102 (2010).
[46] V. G. Ruiz, W. Liu, E. Zojer, M. Scheffler, and A. Tkatchenko, Phys. Rev. Lett. **108**, 146103 (2012).
[47] M. J. McGrath, J. I. Siepmann, I.-F. W. Kuo, and C. Mundy, Mol. Phys. **104**, 3619 (2006).
[48] L. Liu, M. Krack, and A. Michaelides, J. Chem. Phys. **130**, 234702 (2009).
[49] J. Hansen and I. McDonald, *Theory of Simple Liquids*, 2nd ed. (Academic, New York, 1986).
[50] G. Kresse and J. Furthmüller, Comput. Mater. Sci. **6**, 15 (1996).
[51] G. Kresse and J. Furthmüller, Phys. Rev. B **54**, 11169 (1996).
[52] G. Kresse and J. Hafner, Phys. Rev. B **47**, 558 (1993).
[53] P. E. Blöchl, Phys. Rev. B **50**, 17953 (1994).
[54] G. Kresse and D. Joubert, Phys. Rev. B **59**, 1758 (1999).
[55] J. P. Perdew, K. Burke, and M. Ernzerhof, Phys. Rev. Lett. **77**, 3865 (1996).
[56] S. Nosé, J. Chem. Phys. **81**, 511 (1984).
[57] S. Nosé, Mol. Phys. **52**, 255 (1984).
[58] X. B. Zhang, Q. L. Liu, and A. M. Zhu, Fluid Phase Equilib. **262**, 210 (2007).
[59] H. Heinz, R. A. Vaia, B. L. Farmer, and R. R. Naik, J. Phys. Chem. C **112**, 17281 (2008).
[60] CP2K Developers Home Page, see http://www.cp2k.org.
[61] J. W. Halley, A. Mazzolo, Y. Zhou, and D. Price, J. Electroanal. Chem. **450**, 273 (1998).
[62] See supplementary material at http://dx.doi.org/10.1063/1.4752235 for illustrations of some of the typical adsorption structures observed in the Au-water interface.
[63] H. R. Zelsman, J. Mol. Struct. **350**, 95 (1995).
[64] A. J. Lock and H. J. Bakker, J. Chem. Phys. **117**, 1708 (2002).
[65] X.-Z. Li, B. Walker, and A. Michaelides, Proc. Natl. Acad. Sci. U.S.A. **108**, 6369 (2011).
[66] J. E. Bertie and E. Whalley, J. Chem. Phys. **40**, 1637 (1964).
[67] P. T. T. Wong and E. Whalley, J. Chem. Phys. **64**, 2359 (1976).
[68] J. E. Bertie and F. E. Bates, J. Chem. Phys. **67**, 1511 (1977).